Journal of Molecular Catalysis A: Chemical 310 (2009) 144–149

Contents lists available at ScienceDirect

Journal of Molecular Catalysis A: Chemical

journal homepage: www.elsevier.com/locate/molcata

Selective hydrogenation of *o*-chloronitrobenzene (*o*-CNB) over supported Pt and Pd catalysts obtained by laser vaporization deposition of bulk metals

Lingchao Jiang, Huizi Gu, Xingzhong Xu, Xinhuan Yan*

State Key Laboratory Breeding Base of Green Chemistry-Synthesis Technology, Zhejiang University of Technology, Hangzhou, 310014 Zhejiang, PR China

ARTICLE INFO

Article history:
Received 11 January 2009
Received in revised form 31 May 2009
Accepted 5 June 2009
Available online 16 June 2009

Keywords:
Platinum
Palladium
Laser vaporization deposition
o-Chloronitrobenzene
Liquid phase hydrogenation

ABSTRACT

Carbon nanotubes (CNTs), γ-alumina (γ-Al_2O_3) and silica (SiO_2) supported Pt and Pd catalysts were produced by laser vaporization deposition of respective bulk metals. The catalysts were characterized by inductive coupled plasma emission spectrometer (ICP), X-ray photoelectron spectroscopy (XPS) and transmission electron microscopy (TEM). The catalytic properties of the catalysts were investigated in the liquid phase hydrogenation of *o*-chloronitrobenzene (*o*-CNB) to *o*-chloroaniline (*o*-CAN) under 333 K and 1.0 MPa hydrogen pressure. The results show that the catalytic properties are greatly affected by the supports. Pt/CNTs catalyst exhibits the best catalytic performance among the Pt-based catalysts, producing *o*-CAN with 99.6% selectivity at complete conversion. Pd/CNTs catalyst exhibits the best catalytic performance among the Pd-based catalysts, giving *o*-CAN with 95.2% selectivity at complete conversion. For Pt-based catalysts, geometric effect and the textures and properties of the supports play important roles on catalytic properties. On the other hand, geometric effect, electronic effect and the textures and properties of the supports simultaneously influence the catalytic properties of the Pd-based catalysts. In addition, hydrogenolysis of the C–Cl bond can be well inhibited over all catalysts prepared by laser vaporization deposition.

1. Introduction

Aromatic haloamines are important intermediates in the chemistry of dyes, drugs, herbicides and pesticides. The traditional synthesis routes are usually harmful to the environment. "Green" syntheses based on catalytic hydrogenation of the corresponding halogenated nitro compounds are the most common method used currently [1–4]. However, hydrogenation is often companied by hydrodehalogenation, resulting in low selectivity to haloamines. Special catalyst has been proposed as a method for reducing hydrodehalogenation [5,6]. The catalysts generally employed in such reactions are supported Pd [7,8] and supported Pt [9–11] catalysts. Over the last decades, many studies focused on preparation of supported noble metal catalysts. Supported Pt and Pd catalysts were usually prepared by chemical methods [9,12,13], such as impregnation, chemical reduction and so on. Chemical methods were complicated and there are so many factors affecting the catalytic properties during preparation process. In recent years, laser technology was gradually applied in preparation of supported catalysts (physical method). Rousset et al. [14,15] have prepared γ-Al_2O_3 supported Pt, Pd and Pt–Pd catalysts by laser vaporization of respective bulk metals, used for the hydrogenation of toluene and tetralin, and obtained good results.

A number of parameters have been shown [16,17] to influence the activity and selectivity for the hydrogenation of halogenated nitrobenzene in liquid phase, such as noble metal particles size and loading, solvent and the incorporation of a second metal. One more important consideration is the catalyst support. The primary roles of support are to finely disperse and stabilize small metallic particles and thus provide access to a lager number of catalytically active atoms than the corresponding bulk metal [18]. In this paper, a promising support (CNTs) and classical supports (γ-Al_2O_3 and SiO_2) are selected, and supported Pt and Pd catalysts were produced by laser vaporization deposition of bulk metals. Herein the electronic structure and microstructure of the catalysts were extensively investigated by means of high-resolution X-ray photoelectron spectrometer and transmission electron microscope, respectively, while their catalytic performance was evaluated using selective hydrogenation of *o*-chloronitrobenzene under 333 K and 1.0 MPa hydrogen pressure as a probe reaction. We found that the supports have a significant influence on the metal dispersion and the

* Corresponding author. Tel.: +86 571 88320791; fax: +86 571 88320791.
E-mail address: xinhuanyan139@hotmail.com (X. Yan).

1381-1169/$ – see front matter © 2009 Elsevier B.V. All rights reserved.
doi:10.1016/j.molcata.2009.06.009

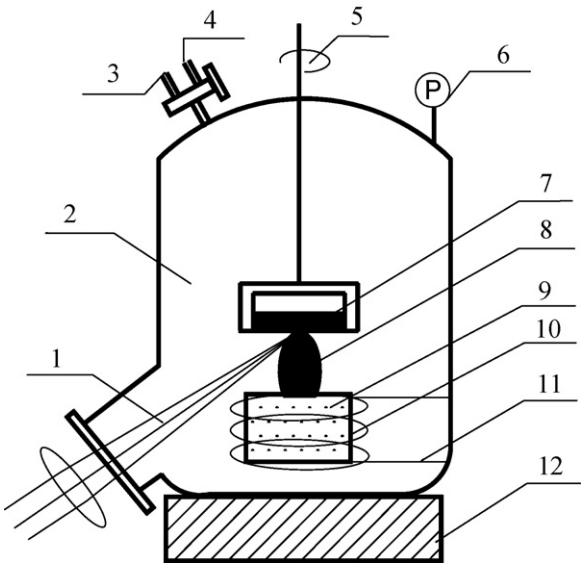

Fig. 1. The system of laser vaporization deposition. (1) Laser; (2) chamber; (3) N_2 cylinder; (4) vacuum pump; (5) stirrer; (6) vacuum meter; (7) metallic rod; (8) plasma; (9) support; (10) quartz dish; (11) strip heater; (12) magnetic stirrer.

particles size, and the catalytic properties of the hydrogenation of *o*-chloronitrobenzene.

2. Experimental

2.1. Preparation of catalysts

Carbon nanotubes (CNTs, SA = 132 m^2/g, Fe 0.004 *wt%* before treated with concentrated nitric acid, Zhejiang university), γ-alumina (γ-Al_2O_3, SA = 238 m^2/g, Zhejiang Zhoushan Mingri Technology Co., Ltd.) and silica (SiO_2, SA = 200 m^2/g, Zhejiang Zhoushan Mingri Technology Co., Ltd.) were used as the catalyst supports.

Pt/CNTs catalyst was prepared by laser vaporization deposition of bulk Pt metal. The deposition system designed by us, is shown in Fig. 1 [19]. A quantity of CNTs pretreated with concentrated nitric acid for overnight (Fe not detectable analyzed by ICP) was placed in the quartz dish at the bottom of the chamber, and agitated by the magnetic stirrer. After N_2 purging to replace air in the chamber for 6 times, the quartz dish was heated to 873 K, and pumped to 300 Pa. Afterwards, a pulsed Nd:YAG (LYD-MC8B, Beijing North Rhine Photoelectric Technology Co., Ltd.) laser of 250 V was focused on a rolling rod of bulk Pt (99.5% purity, Shanghai Jiushan Chemical Co., Ltd.) and a plasma was formed. The plasma was oriented and deposited onto the surface of CNTs and nucleated to form metallic clusters. Thus, the Pt/CNTs (0.5 g per batch) catalyst was obtained.

The preparation of Pt/γ-Al_2O_3 (1.2 g per batch), Pt/SiO_2 (1.2 g per batch), Pd/CNTs (0.5 g per batch), Pd/γ-Al_2O_3 (1.2 g per batch) and Pd/SiO_2 (1.2 g per batch) catalysts are similar to that of Pt/CNTs catalyst (bulk Pd metal, 99.5% purity, Shanghai Jiushan Chemical Co., Ltd.).

2.2. Catalyst characterization

BET surface area was measured by nitrogen volumetric adsorption (BET, Micromeritics ASAP 2010) at 78 K. Prior to measurement, the samples were degassed to 0.1 Pa at 100° for 5–8 h. The surface areas were calculated in a relative pressure range $0.05 < p/p_0 < 0.2$.

The metal loading of the catalysts were analyzed by inductive coupled plasma emission spectrometer (ICP, Thermo Jarrell IRIS-Intrepid). In general, the weighted samples were dissolved in chloroazotic acid to extract the metal from the supports, filtrated, and diluted with distilled water and then the resulting solution was analyzed by the ICP method.

XPS measurements were performed on a Thermo ESCALAB 250 Axis Ultra spectrometer using a monochromatic Al K_α radiation ($h\nu$ = 1486.6 eV). Slight Ar^+ sputtering was employed to remove surface impurities. All binding energy (BE) values were calibrated by using the value of contaminant carbon (C 1s = 284.6 eV) as a reference.

Metal particles size and shape were assessed by transmission electron microscopy analysis. The experiments were performed on a JEOL JEM-200CX transmission electron microscope. In order to obtain samples for TEM characterization, the as-obtained powders were dispersed in ethanol by ultrasonication. A drop of the solution was then deposited onto a thin holey-carbon film supported on a copper microscopy grid and left to dry.

2.3. Catalytic hydrogenation and analysis [20]

Hydrogenation of *o*-CNB was carried out in a 500-mL stainless steel autoclave with a thermocouple and a magnetic stirring bar. A predetermined quantity of *o*-CNB (5 g), ethanol (100 mL) and catalyst were taken. The autoclave was purged with pure hydrogen 5 times to replace air and then was pressurized to 1.0 MPa. The autoclave was heated, stirring started and the reaction time accounted. At the end of the reaction, the autoclave was cooled by flowing water to quench the reaction. The reaction products were analyzed by GC-9790 equipped with a FID detector and an SE-30 capillary column. The oven temperature was 433 K, injector temperature 493 K and detector temperature 533 K.

3. Results and discussions

3.1. BET surface area and metal loading

The BET surface area and the metal loading of the supported Pt and Pd catalysts obtained from BET and ICP measurements, respectively, are gathered in Table 1. The BET surface areas of the supports were slightly decreased after deposition with Pt and Pd for all the Pt-based and Pd-based catalysts. These results above suggest that Pt and Pd have been located on the outer surfaces of the supports. The metal loading of Pt/CNTs, Pt/γ-Al_2O_3, Pt/SiO_2, Pd/CNTs,

Table 1
BET surface area and metal loading of the Pt-based and the Pd-based catalysts.

Catalysts	BET area (m^2 g^{-1})	Metal loading (*wt%*)
Pt/CNTs	129	0.50
Pt/γ-Al_2O_3	230	0.47
Pt/SiO_2	186	0.51
Pd/CNTs	127	0.52
Pd/γ-Al_2O_3	228	0.50
Pd/SiO_2	183	0.49

Table 2
Binding energies (BE) of Pt $4f_{7/2}$ and Pd $3d_{5/2}$ for the Pt-based and the Pd-based catalysts, respectively, measured by XPS.

Catalysts	Binding energy (eV)	
	Pt $4f_{7/2}$	Pd $3d_{5/2}$
Bulk Pt	71.0	
Pt/CNTs	71.4	
Pt/γ-Al_2O_3	71.4	
Pt/SiO_2	71.4	
Bulk Pd		335.0
Pd/CNTs		336.1
Pd/γ-Al_2O_3		335.9
Pd/SiO_2		335.8

Pd/γ-Al_2O_3 and Pd/SiO_2 catalysts are 0.50 *wt%*, 0.47 *wt%*, 0.51 *wt%*, 0.52 *wt%*, 0.50 *wt%* and 0.49 *wt%*, respectively.

3.2. Electronic structure investigation

The XPS results of the Pt-based and the Pd-based catalysts are gathered in Table 2. It shows that the valence state of Pt and Pd are zero. The core level binding energies for Pt/CNTs, Pt/γ-Al_2O_3 and Pt/SiO_2 catalysts and bulk Pt metal are compared. Shift of the Pt $4f_{7/2}$ level to higher binding energy than bulk Pt metal is observed for the Pt-based catalysts. More interestingly, the positive shift of about 0.4 eV is observed for all the Pt-based catalysts. As pointed out by Dicenzo and Wertheim [21], the binding energy is, without exception, higher in clusters than in the bulk. The observed core level shift for Pt clusters agrees with the result reported by Zhao et al. [22], who measured positive shifts on Pt clusters, having a size similar to our clusters. Therefore, we can speculate that the positive shift of binding energies is attributed to the size effect, and the metal–support interaction is negligible for the Pt-based catalysts. The core level binding energies for Pd/CNTs, Pd/γ-Al_2O_3 and Pd/SiO_2 catalysts and Pd bulk are also compared in Table 2. The positive shift of binding energies for Pd $3d_{5/2}$ is in the order

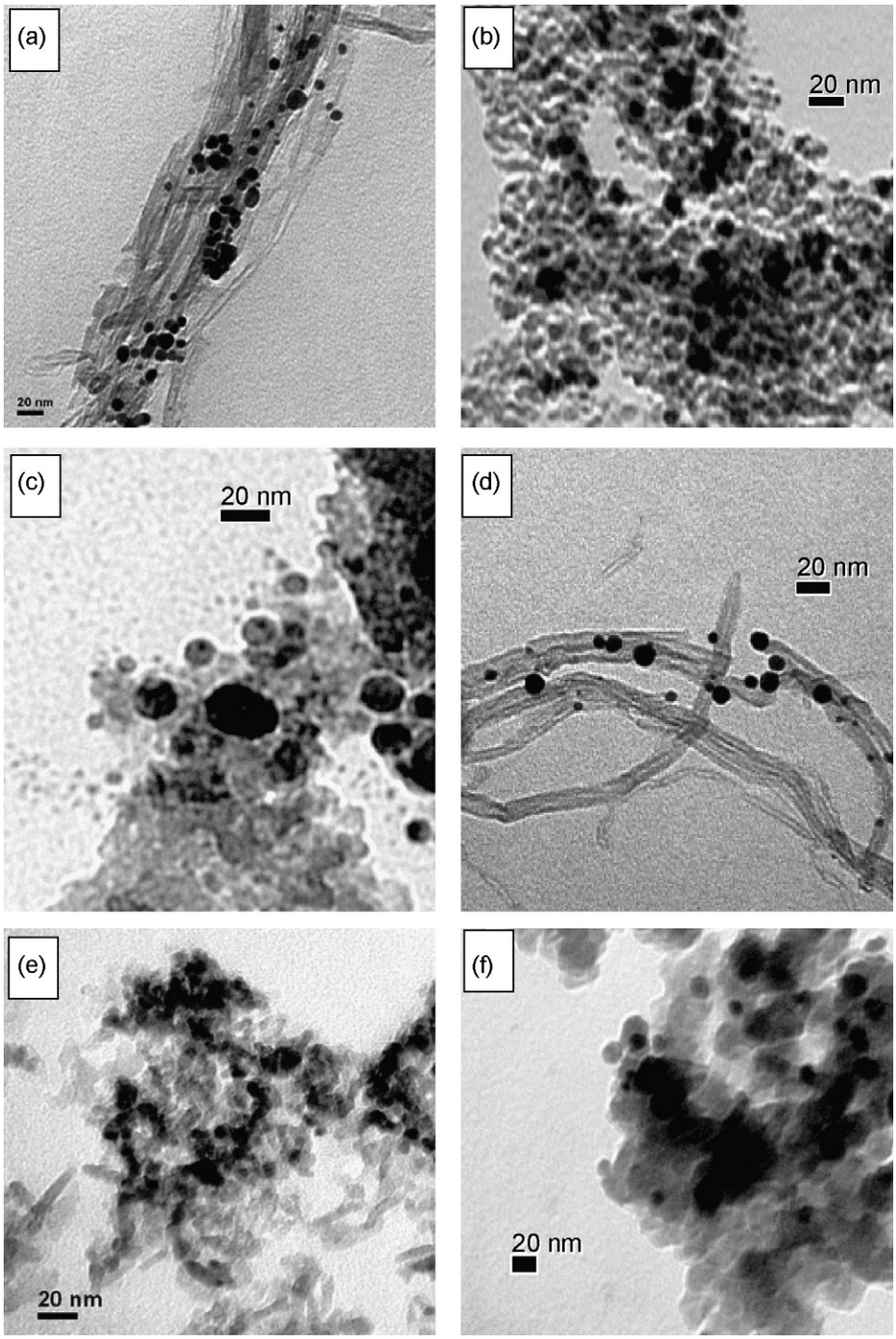

Fig. 2. TEM images of the catalysts. (a) Pt/CNTs, (b) Pt/γ-Al_2O_3, (c) Pt/SiO_2, (d) Pd/CNTs, (e) Pd/γ-Al_2O_3 and (f) Pd/SiO_2.

Pd/CNTs > Pd/SiO_2 > Pd/γ-Al_2O_3. We can speculate that the positive shift of binding energies is attributed to the size effect and the metal–support interaction for the Pd-based catalysts. The results discussed above show that the metal–support interaction is dependent on the metal type. The ionization potential of Pd metal (8.3 eV) is smaller than that of Pt metal (9.0 eV) [23], making the electron transfer of Pd metal more easy.

3.3. Microstrcture investigation

The TEM images of the Pt-based and the Pd-based catalysts are presented in Fig. 2. The TEM images clearly show that Pt and Pd particles are located on the outer surface of the supports. The representative TEM images of Pt/CNTs, Pt/Al_2O_3 and Pt/SiO_2 catalysts shown in Fig. 2a–c reveal pseudo-spherical particles evenly distributed over the outer surface of the supports. It is apparently shown that Pt particles deposited on the outer surface of CNTs are smaller and that the variation in particles size is narrower than those deposited on γ-Al_2O_3 and SiO_2. The respective values of the size range are as follows: Pt/CNTs, 3–12 nm; Pt/γ-Al_2O_3, 4–15 nm; Pt/SiO_2, 6–20 nm. TEM images of Pd/CNTs, Pd/Al_2O_3 and Pd/SiO_2 catalysts are given in Fig. 2d–f. Inspection of wide regions of CNTs supported Pd catalyst shows that Pd metal is evenly dispersed on the entire outer surface of CNTs, and in this case the Pd particles are significantly smaller on average than those deposited on γ-Al_2O_3 and SiO_2. The size of Pd particles increases sharply in the order Pd/CNTs < Pd/γ-Al_2O_3 < Pd/SiO_2, and large aggregates are observed on γ-Al_2O_3 and SiO_2. These results above indicate that the metal dispersion and the particles size are greatly influenced by the supports.

It is clear that the surface area is in the order γ-Al_2O_3 > SiO_2 > CNTs. However, the external surface of CNTs is comparable to that of γ-Al_2O_3 and SiO_2 where a large part of the surface area is attributed to micropores. Large external surface area of supports is favorable for improving metal dispersion. Metal dispersion is not only associated with external surface area of the supports but also connected with their textures and properties, and the metal–support interaction. Supports γ-Al_2O_3 and SiO_2 possess disordered porous network structure, while CNTs [24] have graphitic structure with basal planes exposed. The shortcoming of disordered porous network structure is obvious. Active phase hardly accessed the pores when the supported catalysts were obtained by laser vaporization deposition. The exposed graphitic planes of CNTs make outer surface accessible for the active phase. Metal particles crystallize and the size is controlled by the nuclei number and growth rate. Metal particles obtained by laser vaporization deposition moved more easily on the outer surface of CNTs, which have homogeneous properties. However, γ-Al_2O_3 and SiO_2 have a number of acid centers on the outer surface. Therefore, metal particles are homogeneously and separately dispersed on the outer surface of CNTs, while those deposited on the outer surface of γ-Al_2O_3 and SiO_2 are inhomogeneous. Metal particles on CNTs are smaller than those on γ-Al_2O_3 and SiO_2. A peculiar metal–support interaction could significantly modify metal dispersion, leading to a possible positive influence on the final metal particles dispersion. The Pt–support interaction is negligible, but the Pd–support interaction is in the order Pd/CNTs > Pd/γ-Al_2O_3 > Pd/SiO_2 (Table 2). Such a relatively strong interaction between Pd clusters and CNTs could give rise to the relatively high Pd dispersion on the surface of CNTs leading to high final Pd particles dispersion [12]. The Pd dispersion on the outer surface of γ-Al_2O_3 and SiO_2 are inhomogeneous due to lower Pd–support interaction and homogeneous properties of the support leading to Pd particles aggregated. Baker and co-workers [25,26] have reported that Ni particles supported on carbon nanofibers (CNFs) adopt dramatically different sizes and morphological properties compared to those observed on classical supports such as alumina and silica due to a strong metal–support interaction between Ni particles and CNFs.

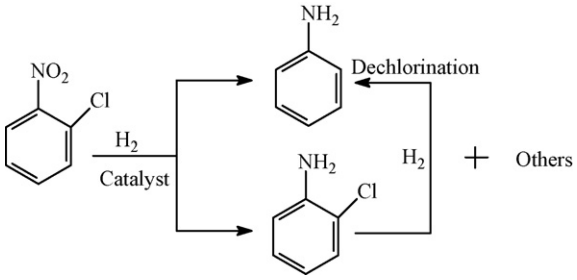

Scheme 1. The process of the hydrogenation of *o*-CNB.

3.4. Catalyst activity/selectivity

3.4.1. Pt-based catalysts

The hydrogenation of *o*-CNB was used to test the catalytic properties of the Pt-based and Pd-based catalysts. The hydrogenation of *o*-CNB to give *o*-chloroaniline (*o*-CAN) as the main product is shown in Scheme 1. Aniline (AN) is the main by-product. Other detectable by-products include nitrobenzene (NB), *o*-chloronitrosobenzene (*o*-CNSB) and azobenzene. The effect of the supports on the hydrogenation of *o*-CNB over Pt-based catalysts has been investigated, and the results are listed in Table 3. It can be seen that the supports have an obvious influence on the catalytic activity of the Pt-based catalysts on the hydrogenation of *o*-CNB. Pt/CNTs catalyst exhibits the best catalytic activity. The catalytic activity decreases sharply in the order Pt/CNTs > Pt/γ-Al_2O_3 > Pt/SiO_2. It is well known that the catalytic activity is influenced by geometric and/or electronic effect. The Pt particles of Pt/CNTs catalyst are smaller than those of Pt/γ-Al_2O_3 and Pt/SiO_2 catalysts (Fig. 2a–c). The electronic interaction between Pt clusters and the supports is negligible (Table 2). Thus, we can speculate that geometric effect on the catalytic activity is considerable. It is well known [27] that the rate-determining step of heterogeneously catalytic reaction is a nucleophilic attack of hydride ion, produced by dissociated adsorption of hydrogen molecules on the metal (Pt) surface, on the N=O bond of the nitro group. Higher Pt dispersion and smaller Pt particles of Pt/CNTs catalyst promote the contact of the nitro group of *o*-CNB with the active sites. The diffusion of reactants towards the active sites located on the outer surface of CNTs is easier than that on γ-Al_2O_3 and SiO_2 because of the exposed basal planes of CNTs. Thus, the N=O bond is favorably attacked by hydride ion adsorbed on the active sites of Pt/CNTs catalyst, resulting in higher catalytic activity.

However, a more significant difference was observed for Pt-based catalysts in terms of the selectivity to *o*-CAN in Table 3. The selectivity to *o*-CAN is almost equivalent over all Pt-based catalysts. The supports have no distinct effect on the selectivity to *o*-CAN. This is inconsistent with the results obtained by Coq et al. [28], who have reported that the supports have obvious effect on the selectivity to *p*-CAN over the Pt-based catalysts obtained by chemical ways. Coq et al. [11] also have reported that higher Pt dispersion and smaller Pt particles exhibit higher selectivity to *o*-CAN. The rate-determining step of the hydrodechlorination of *o*-CNB is a nucleophilic attack of hydride ion on the C–Cl bond. The properties of hydrogen chemisorped on Pt particles are linked to the electronic state of the Pt active sites. Therefore, we can speculate that the invariant selectivity to *o*-CAN over all Pt-based catalysts is linked to the negligible metal–support interaction. The invariant selectivity to *o*-CAN may also be linked to the textures and properties of the supports. The complete absence of any microporosity was found on CNTs, which could modify residence time of the reactant and product and their

Table 3
Comparison between reaction data of the Pt-based and Pd-based catalysts on the hydrogenation of *o*-CNB.

Catalysts	Average rate[a] ($mol_{o\text{-CNB}}\ mol_{metal}^{-1}\ min^{-1}$)	Conversion (%) (time, min)	Selectivity (%)	
			AN	*o*-CAN
Pt/CNTs	131.0	100 (105)	0.4	99.6
Pt/γ-Al_2O_3	58.1	97.3 (120)	0.6	99.4
Pt/SiO_2	35.7	79.5 (180)	0.4	99.6
Pd/CNTs	141.2	100 (92)	4.3	95.2
Pd/γ-Al_2O_3	59.5	95.2 (120)	9.4	89.1
Pd/SiO_2	36.5	85.8 (180)	7.9	91.2

Reaction condition: m (*o*-CNB) = 5 g; V (EtOH) = 150 mL; P (H_2) = 1.0 MPa; reaction temperature = 333 K; m (Pt/CNTs) = 0.09 g; m (Pt/γ-Al_2O_3) = 0.15 g; m (Pt/SiO_2) = 0.15 g; m (Pd/CNTs) = 0.05 g; m (Pd/γ-Al_2O_3) = 0.09 g; m (Pd/SiO_2) = 0.12 g.

[a] The average reaction rate, $mol_{o\text{-CNB}}\ mol_{metal}^{-1}\ min^{-1}$, calculated from the amount of *o*-CNB consumption.

adsorption. The lower concentration of oxygenated groups on CNTs surface compared to their high concentration on γ-Al_2O_3 and SiO_2 surface could also influence in a significant manner the selectivity to *o*-CAN by modifying the adsorption mode of reactant. Finally, it should be noted that an interaction would be possible between the N=O bond of *o*-CNB and the exposed graphite planes associated with a cloud of delocalized π-electrons of CNTs, which also could improve the selectivity to *o*-CAN.

3.4.2. Pd-based catalysts

The effect of the supports on the hydrogenation of *o*-CNB over Pd-based catalysts has been investigated, and the results are listed in Table 3. The results clearly pointed out the superiority of CNTs supported Pd catalysts versus γ-Al_2O_3 and SiO_2 in terms of the catalytic activity and the selectivity to *o*-CAN. Pd/CNTs catalyst exhibits the best catalytic activity and the highest selectivity to *o*-CAN (95.2%). The catalytic activity and selectivity to *o*-CAN simultaneously decrease in the order Pd/CNTs > Pd/γ-Al_2O_3 > Pd/SiO_2. The Pd particles of Pd/CNTs catalyst are smaller than those of Pd/γ-Al_2O_3 and Pd/SiO_2 catalysts, and large aggregates are observed on the surface of Pd/γ-Al_2O_3 and Pd/SiO_2 catalysts (Fig. 2d–f). The metal–support interaction is in the order Pd/CNTs > Pd/SiO_2 > Pd/γ-Al_2O_3 (Table 2). Thus, we can speculate that the excellent catalytic properties of the Pd/CNTs catalysts are explained by the geometric and electronic effects and the textures and properties of CNTs. The effect of the supports on the catalytic activity of the Pd-based catalysts is similar to that on the Pt-based catalysts. Different results in terms of the effect of the supports on the selectivity to *o*-CAN are observed compared to the Pt-based catalysts (Table 3). The *o*-CAN selectivity results over Pd-based catalysts are similar to those obtained by Planeix et al. [29], who have reported that Ru/CNTs catalyst has higher cinnamyl alcohol selectivity in the hydrogenation of cinnamaldehyde than Ru/Al_2O_3 and Ru/C catalysts. This may be attributed to the higher dispersion of Pd and stronger Pd–support interaction for Pd/CNTs catalyst. Coq et al. [30] have reported that the dispersion of Pd affects the hydrogenolysis of C–Cl bond in chlorobenzene, larger Pd particles being more active for hydrodechlorination. The existence of a peculiar metal–support interaction between Pd particles and the supports, i.e. electronic modification through the electron transfer between Pd metal and the supports modifies the adsorption and selectivity of the product. A lower electronic density at the Pd sites of Pd/CNTs catalyst due to the electron transfer between the graphite structure of CNTs and Pd particles lowers the negative charge of hydrogen chemisorped on the active sites of Pd/CNTs catalyst [31]. Generally, this inhibits hydrogenolysis of the C–Cl bond in *o*-CNB and *o*-CAN, resulting in the highest selectivity to *o*-CAN over Pd/CNTs catalyst.

3.4.3. Hydrogenolysis of the C–Cl bond in o-CAN inhibited

The effect of time on the conversion of *o*-CNB and the selectivity to *o*-CAN is shown in Fig. 3. It can be seen from Fig. 3 that the selectivity to *o*-CAN is constant with time going over Pt-based

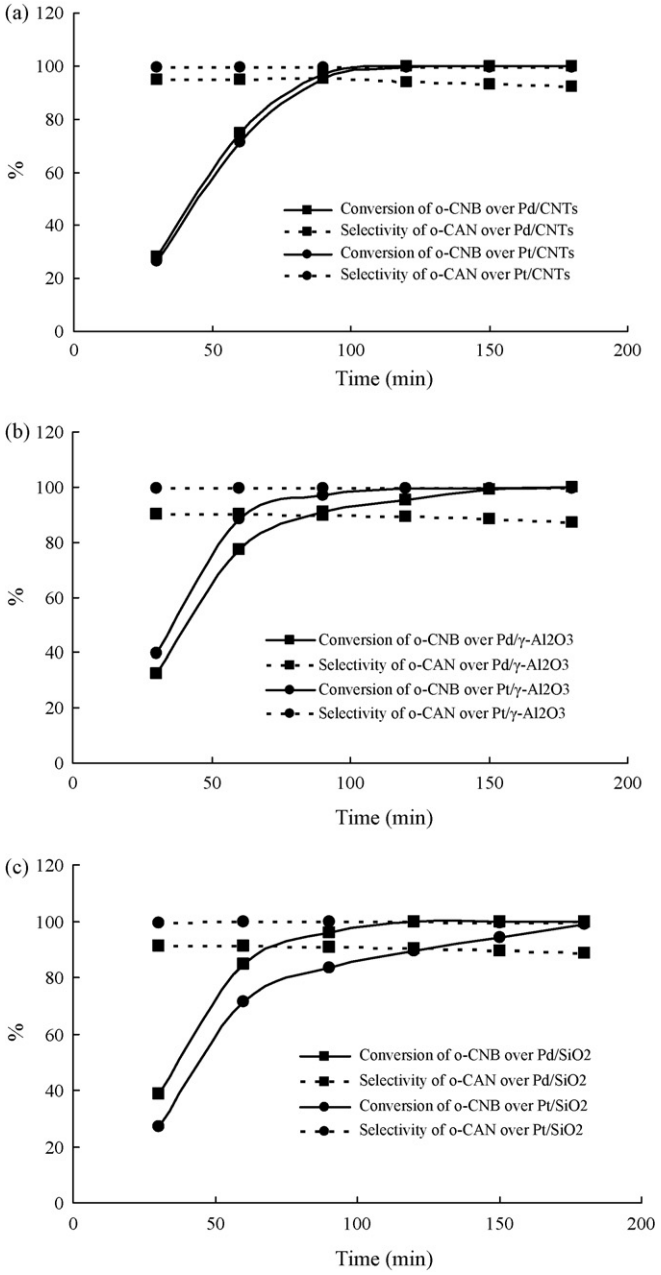

Fig. 3. Effect of reaction time on the conversion and the selectivity to *o*-CAN. (a) Pd/CNTs (0.05 g) and Pt/CNTs (0.09 g); (b) Pd/γ-Al_2O_3 (0.09 g) and Pt/γ-Al_2O_3 (0.15 g); (c) Pd/SiO_2 (0.15 g) and Pt/SiO_2 (0.21 g). Reaction condition: m (*o*-CNB) = 5 g; V (EtOH) = 150 mL; P (H_2) = 1.0 MPa; reaction temperature = 333 K; reaction time = 180 min.

catalysts, and that the selectivity to *o*-CAN slightly decreases with time over Pd-based catalysts. It is well known that there are two pathways for hydrodechlorination during the hydrogenation of *o*-CNB, hydrogenolysis of C–Cl bond in *o*-CNB and hydrogenolysis of C–Cl bond in *o*-CAN, respectively (Scheme 1). The results obtained in the laboratory have shown that active phase located on the outer surface of the supports exhibits an extremely high ability to inhibit the further hydrogenation of *o*-CAN, namely hydrogenolysis of the C–Cl bond in *o*-CAN. This could be attributed to several factors: (i) Metal clusters were deposited on the outer surface of the supports, according to the laser vaporization deposition process, BET results (Table 1) and TEM results (Fig. 2), which modifies the adsorption of *o*-CAN. The N=O hydrogenation product (*o*-CAN) was rapidly desorbed from the active sits on the outer surface of the catalysts. The re-adsorption of *o*-CAN may not occur on the active sites regardless of support. Thus, the residence time of *o*-CAN on the surface of catalyst is shortened. (ii) The electron-deficient state of the metal particles may inhibit the C–Cl bond in the contact of *o*-CAN with the active sites. (iii) For Pd-based catalysts, the size effect and the metal–support interaction induce the electron-deficient state of the Pd particles, which lowers negative charge of the hydrogen. Generally, this inhibited the C–Cl bond in *o*-CAN attracted by hydride ion, and hydrogenolysis of the C–Cl bond in *o*-CAN is inhibited.

4. Conclusions

It is clear that laser vaporization deposition is a simple approach to preparation of supported Pt and Pd catalysts. The metal–support interaction for the Pt-based catalysts is negligible, but the metal–support interaction for the Pd-based interaction is in the order Pd/CNTs > Pd/γ-Al_2O_3 > Pd/SiO_2. The supports have a significant influence on the metal dispersion and the particles size. The hydrogenation results show the superiority of CNTs over γ-Al_2O_3 and SiO_2 in terms of the catalytic activity and the selectivity to *o*-CAN. The effect of the supports may be interpreted by geometric effect and the textures and properties of the supports for the Pt-based catalysts. However, the effect of the supports may be interpreted by geometric effect, electronic effect and the textures and properties of the supports for the Pd-based catalysts. In addition, hydrogenolysis of the C–Cl bond in *o*-CAN is well inhibited over supported Pt and Pd catalysts obtained by laser vaporization deposition due to the metal particles deposited on the outer surface of the supports. Such catalysts can be potentially applied in several reactions, and will probably open a new era in the field of nanosized catalytic materials with high selectivity, especially in liquid-phase medium where the metal particles deposited on the outer surface of support can lower mass transfer limitation.

Acknowledgements

Financial support of the Natural Science Foundation of Zhejiang (project Y404002) and the fund of the Science and Technology of Zhejiang (project 2005C21054) are gratefully acknowledged.

References

[1] B. Coq, A. Tijani, F. Figueras, J. Mol. Catal. 71 (1992) 317–333.
[2] Q. Xu, X.M. Liu, J.R. Chen, R.X. Li, X.J. Li, J. Mol. Catal. A 260 (2006) 299–305.
[3] M.H. Liu, W.Y. Yu, H.F. Liu, J.M. Zheng, J. Colloid Interface Sci. 214 (1999) 231–237.
[4] Z.H. Yu, Z.X. Li, J.L. Tian, J. Mol. Catal. A 265 (2007) 258–267.
[5] P.N. Rylander, M. Kilroy, V. Coven, Engelhard Ind. Technol. Bull. 6 (1965) 11–16.
[6] W.P. Dunworth, F.F. Nord, J. Am. Chem. Soc. 74 (1952) 1459–1462.
[7] Z.K. Yu, S.J. Liao, Y. Xu, B. Yang, D.R. Yu, J. Chem. Soc. Chem. Commun. 11 (1995) 1155–1156.
[8] L.M. Sikhwivhilu, N.J. Coville, B.M. Pulimaddi, J. Venkatreddy, V. Vishwanathan, Catal. Commun. 8 (2007) 1999–2006.
[9] J.L. Zhang, Y. Wang, H. Ji, Y.G. Wei, N.Z. Wu, B.J. Zuo, Q.L. Wang, J. Catal. 229 (2005) 114–118.
[10] X.X. Han, R.X. Zhou, G.H. Lai, X.M. Zheng, Catal. Today 93–95 (2004) 433–437.
[11] B. Coq, A. Tijani, F. Figueras, J. Mol. Catal. 68 (1991) 331–345.
[12] J.P. Tessonnier, L. Pesant, G. Ehret, M.J. Ledoux, C. Pham-Huu, Appl. Catal. A 288 (2005) 203–210.
[13] X.X. Han, Q. Chen, R.X. Zhou, J. Mol. Catal. A 277 (2007) 210–214.
[14] J.L. Rousset, L. Stievano, F.J. Cadete Santos Aires, C. Geantet, A.J. Renouprez, M. Pellarin, J. Catal. 197 (2001) 335–343.
[15] J.L. Rousset, L. Stievano, F.J. Cadete Santos Aires, C. Geantet, A.J. Renouprez, M. Pellarin, J. Catal. 202 (2001) 163–168.
[16] X.D. Wang, M.H. Liang, J.L. Zhang, Y. Wang, Curr. Org. Chem. 11 (2007) 299–314.
[17] B. Coq, F. Figueras, Coord. Chem. Rev. 178–180 (1998) 1753–1783.
[18] E. Auer, A. Freund, J. Pietsch, T. Tack, Appl. Catal. A 173 (1998) 259–271.
[19] X.Z. Xu, J.F. Yang, X.N. Li, X.H. Yan, Acta Phys. Chim. January Sin. 24 (2008) 121–126.
[20] X.H. Yan, J.Q. Sun, Y.H. Xu, J.F. Yang, Chin. J. Catal. 27 (2006) 119–123.
[21] S.B. Dicenzo, G.K. Wertheim, Comments Solid State Phys. 11 (1985) 203–219.
[22] Z.J. Zhao, F. Liu, L.M. Qiu, L.Z. Zhao, Acta Phys. Chim. January Sin. 24 (2008) 001–009.
[23] R.C. Weast (Ed.), CRC Handbook of Chemistry and Physics, 70th ed., CRC Press, Boca Raton, FL, 1989–1990, pp. E80–E81.
[24] C.H. Li, Z.X. Yu, K.F. Yao, S.F. Ji, J. Liang, J. Mol. Catal. A 226 (2005) 101–105.
[25] A. Chambers, T. Nemes, N.M. Rodriguez, R.T.K. Baker, J. Phys. Chem. B 102 (1998) 2251–2258.
[26] F. Salman, C. Park, R.T.K. Baker, Catal. Today 53 (1999) 385–394.
[27] P. Lu, N. Toshima, Bull. Soc. Jpn. 73 (2000) 751–758.
[28] B. Coq, A. Tijani, R. Dutartre, J. Mol. Catal. 79 (1993) 253–264.
[29] J.M. Planeix, N. Coustel, B. Coq, V. Brotons, P.S. Kumbhar, R. Dutartre, P. Geneste, P. Bernier, P.M. Ajayan, J. Am. Chem. Soc. 116 (1994) 7935–7936.
[30] B. Coq, G. Ferrat, F. Figueras, J. Catal. 101 (1986) 434–445.
[31] V. Kratky, M. Kralik, M. Mecarova, M. Stolcova, L. Zalibera, M. Hronec, Appl. Catal. A 235 (2002) 225–231.